Numerical Solutions of Reflected Shock-Wave Flowfields with Nonequilibrium Chemical Reactions

LEROY L. PRESLEY*
NASA Ames Research Center, Moffett Field, Calif.

AND

RONALD K. HANSON†
Stanford University, Stanford, Calif.

The method of characteristics for a reacting gas is employed to construct the time-dependent, one-dimensional flowfield resulting from the normal reflection of an incident shock wave at the end wall of a shock tube. Nonequilibrium chemical reactions are allowed behind both the incident and reflected shock waves. All of the solutions are evaluated for oxygen, but the general features of the results are representative of any inviscid, nonconducting, and nonradiating diatomic gas. The solutions clearly show that 1) both the incident- and reflected-shock chemical-relaxation times are important in governing the time to attain steady-state thermodynamic properties; and that 2) adjacent to the end wall, a variable-entropy layer develops wherein the steady-state values of all of the thermodynamic variables, except pressure, differ significantly from their corresponding Rankine-Hugoniot equilibrium values.

Nomenclature

a = sound speed at frozen chemistry (cm/sec)
D = dissociation energy (117,960 cal/mole for O_2)
h = enthalpy per initial mole of molecules (cal/mole)
K_c = equilibrium constant (moles/cm^3)
k_d = dissociation rate (cm^3/mole-sec)
k_r = recombination rate (cm^6/mole^2-sec)
O = oxygen atom
O_2 = oxygen molecule
P = pressure (atm, or dynes/cm^2)
p = partial pressure (atm)
R = gas constant (1.987 cal/mole-°K)
R^* = gas constant (82.06 cm^3-atm/mole-°K)
R' = gas constant (2.598×10^6 ergs/g-°K for O_2)
S = entropy per unit mass (cal/g-°K)
T = temperature (°K)
t = time (sec)
U = velocity of incident shock wave relative to end wall (cm/sec)
u = velocity of gas behind reflected shock wave relative to end wall (cm/sec)
V = velocity of reflected shock wave relative to end wall (cm/sec)
v = velocity of gas behind incident shock relative to incident shock (cm/sec)
W = molecular weight of diatomic gas (W = 32 g/mole for O_2)
w = mass rate of production of a chemical species (g/cm^3-sec)
X = arbitrary collision partner
x = distance from shock-tube end wall (cm)
α = degree of dissociation (also mass fraction of atoms, ρ_0/ρ)
β = rate-constant multiplier
δ = derivative along characteristic line
θ_d = characteristic temperature of dissociation (θ_d = 58,960 °K for O_2)
θ_v = characteristic temperature of vibration (θ_v = 2,274°K for O_2)
μ = chemical potential (cal/g)
ρ = mass density (g/cm^3)
[ ] = concentration (moles/cm^3)

Subscripts

eq = equilibrium properties
i = general spatial point behind incident shock wave
k = specific chemical species
1 = ahead of incident-shock wave
2 = behind incident-shock wave
3 = behind reflected-shock wave
30 = behind reflected-shock wave at instant of reflection

Presented as Paper 68-732 at the AIAA Fluid and Plasma Dynamics Conference, Los Angeles, Calif., June 24–26, 1968; submitted December 2, 1968; revision received May 19, 1969. The coding of the computer program for obtaining the results discussed in this paper was performed by E. Williams. Her contribution to this study is very gratefully acknowledged.

* Research Scientist.
† Research Associate, Aeronautics and Astronautics Department. Member AIAA.

Introduction

THE use of shock tubes for studies of high-temperature gasdynamics and nonequilibrium chemical kinetics is well established. Many of these studies have been conducted by observing the gas heated by the reflection of an incident or primary shock wave at the end wall of a shock tube (see, e.g., Johnson and Britton[1]). The well-known advantages of reflected-shock testing are:

1) The temperature behind the reflected-shock wave is increased to roughly twice that behind the incident-shock wave.

2) The gas behind the reflected-shock wave is essentially stationary in laboratory coordinates; thus greater time resolution can be achieved than is obtainable behind incident-shock waves at the same conditions.

However, several phenomena occur behind reflected-shock waves which tend to limit their usefulness to produce a well-defined sample of hot test gas. For the most part, these phenomena give rise to uncertainties in the thermodynamic state of the test gas. Three phenomena occur as a consequence of the side-wall viscous boundary layer that develops behind the incident-shock wave. First, the presence of the boundary layer induces spatially nonuniform properties within the flowfield behind the incident-shock wave, thus causing time-dependent upstream properties for the reflected shock wave. Kamimoto et al.[2] and Rudinger[3] have analyzed this problem with regard to the slow pressure rise often ob-

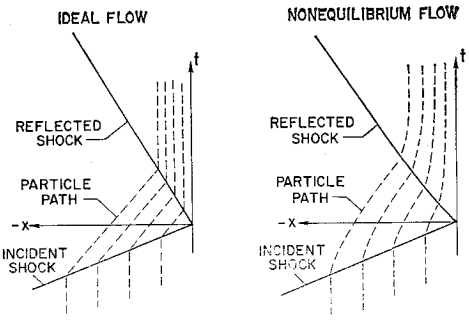

Fig. 1 Comparison of reflected-shock wave x-t diagram for ideal and nonequilibrium flow.

served on the end wall of a shock tube after shock reflection. Second, as the reflected shock propagates back through the side-wall boundary layer, a complicated shock-wave, boundary-layer interaction is initiated. The severity of this interaction increases with increasing molecular complexity. Mark[4] and Strehlow and Cohen[5] have made observations of the bifurcation resulted from the interaction and concluded that it is very small for monatomic gases and sufficiently small for diatomic gases to have little effect on kinetic studies conducted immediately adjacent to the end wall. Third, the side-wall boundary layer causes the incident-shock wave to be curved. On the basis of experimental data, Lin and Fyfe[6] argued that the center displacement of the incident-shock wave is directly proportional to $(r/\rho_1)^{1/2}$, where r is the shock-tube radius and ρ_1 is the initial density. However, the effects of a curved incident-shock wave upon a reflected-shock-wave flowfield are not well understood.

A fourth phenomenon affecting the reflected-shock-wave flowfield arises from the thermal boundary layer that forms on the end wall of the shock tube. Sturtevant and Slachmuylders[7] have studied, both theoretically and experimentally, the effect of the end-wall thermal boundary layer upon the trajectory of the reflected-shock wave. Goldsworthy[8] has obtained expressions for the thickness of the thermal layer on the end wall. Generally, these results show that if the initial pressure is greater than about 1 torr, the effects of the heat transfer upon the flowfield are not significant at distances greater than 1 mm from the end wall.

Since all of the aforementioned phenomena result from viscous or heat-conduction effects, the controlling factors, if not the phenomena themselves, are well understood. Thus, these nonidealities can be minimized by appropriate selection of experimental technique, test conditions, and observation interval. However, an additional problem exists for studies involving nonequilibrium chemical reactions because an adequate theory for predicting the entire flowfield in even an inviscid and nonconducting gas has not been available. This latter aspect of shock-wave reflection is the subject to which this paper is addressed. The general problem is to determine the reflected-shock flowfield when nonequilibrium chemical reactions are present behind both the incident- and reflected-shock waves. The method of characteristics for a one-dimensional reacting gas is employed to obtain numerical solutions.

The closely related problem of reflected-shock flowfields with vibrational nonequilibrium was discussed first qualitatively by Baganoff,[9] with particular emphasis on the vibrational relaxation of CO_2. Johannesen et al.[10] have recently obtained quantitative results for the vibrational relaxation of CO_2 behind reflected-shock waves using the method of characteristics. Many of the general features of these works also appear in the present results. The emphasis of the present work, however, is on defining quantitatively the effect of nonequilibrium *chemical reactions* upon a reflected-shock flowfield. A simple chemical model has been used to show clearly the coupling between the fluid mechanics and chemistry. Once the basic features of a nonequilibrium reflected-shock flowfield are understood, the inclusion of a more complicated chemical model is straightforward.

Method of Analysis

The general problem of finding a solution for a reflected-shock flowfield with nonequilibrium chemical reactions introduces several phenomena that are not considered in the usual equilibrium solutions of reflected-shock properties. For example, nonequilibrium flow behind the incident-shock wave causes curvature of the particle paths in the x-t plane (see Fig. 1) and results in a spatial gradient in all of the fluid and thermodynamic properties behind the incident-shock wave. The reflected-shock wave must propagate back into this nonuniform region; thus its upstream properties are continually changing. As a result of both the time-varying upstream properties, and the nonequilibrium chemical reactions behind the reflected-shock wave, the velocity of the reflected-shock wave is not constant (Fig. 1). In addition, the usual boundary condition of zero flow velocity behind the reflected shock now holds only at the end wall, and the particle paths behind the reflected-shock wave are curved.

From the previous discussion, it is clear that the over-all solution can be divided into two discrete portions: 1) solution of the flow behind the incident-shock wave, and 2) solution of the flow behind the reflected-shock wave. Several assumptions regarding the mathematical model for both solutions are:

1) The gas, which is oxygen, is considered to be thermally perfect.

2) The vibrational energy is assumed to be in equilibrium at the local translational temperature, and is given by a harmonic-oscillator model.

3) Both molecules and atoms are in their ground electronic states.

4) The specific reaction considered is

$$O_2 + X \rightleftarrows 2O + X$$

where X is an arbitrary collision partner, either a molecule or an atom of oxygen.

5) All transport processes have been neglected.

6) The end wall is chemically inert.

Although the previous assumptions are somewhat restrictive insofar as providing a physically realistic gas model, it should be recalled that the primary purpose of this study is to show the coupling of nonequilibrium chemical reactions and fluid mechanics in a reflected-shock flowfield. Adoption of a more realistic gas model would produce secondary effects upon the results shown in this paper.

Incident-Shock Solution

The solution of incident-shock-wave flowfields with finite-rate chemistry is straightforward. The set of equations used is presented below primarily for the purpose of completeness.

Conservation equations

Mass:

$$\rho_1 U = \rho_i v_i \tag{1}$$

Momentum:

$$P_1 + \rho_1 U^2 = P_i + \rho_i v_i^2 \tag{2}$$

Energy:

$$h_1 + (\tfrac{1}{2})U^2 = h_i + (\tfrac{1}{2})v_i^2 \tag{3}$$

Equations of state

Thermal:

$$P_i = (1 + \alpha)_i \rho_i (R^*/W) T_i \tag{4}$$

Caloric:

$$h_i = [(7 + 3\alpha_i)/2]RT_i + [(1 - \alpha_i)R\theta_v/(e^{\theta_v/T_i} - 1)] + \alpha_i D \quad (5)$$

Rate equation

$$D\alpha_i/Dt = -W/\rho(-k_d[O_2][X] + k_r[O]^2[X]) \quad (6)$$

where

$$k_r = \beta A T^m$$
$$k_d = K_c k_r$$
$$K_c = 0.666\ T^{1/2}e^{-\theta_d/T}(1 - e^{-\theta_v/T})$$

The rate constant k_r used in the foregoing expressions represents a best fit of several experimental studies; see, for example, Green and Toennies.[11] The particular values of A and m selected are 7.29×10^{21} (cm^6/mole^2-sec) and -2, respectively; β is a multiplier for conveniently varying the magnitude of the rate constant. The simplified expression for the equilibrium constant K_c was derived from statistical mechanics.

The previous set of equations is solved at each point i in the incident-shock flowfield, subject to the following boundary conditions: 1) no dissociation occurs across the shock front; and 2) equilibrium is reached when $D\alpha/Dt$ goes to zero.

Flowfield properties throughout the incident-shock nonequilibrium zone must be retained since they provide the time-varying upstream conditions for the reflected-shock wave.

Reflected-Shock Solution

The entire flowfield behind the reflected-shock wave is constructed using the method of characteristics. Derivations of the appropriate characteristic equations have appeared elsewhere (see, for example, the papers by Ferri[12] and Chu[13]), so only the final form of the equations used in this analysis will be shown below. In addition, since the complete calculational procedure is very detailed and lengthy, only a brief description of the logic of the numerical solution will be presented herein.

Basic equations

The equations for the change in pressure and velocity along characteristic Mach lines in a reacting gas are identical to those for a nonreacting gas except for an added term, i.e.,

$$(1/\rho a^2)(\delta P/\delta t) \pm (1/a)(\delta u/\delta t) = G/\rho \quad (7a,7b)$$

where the plus and minus signs [Eqs. (7a) and (7b)] correspond to the right- and left-running characteristics respectively, and δ is the derivative along the characteristic line. The added term G/ρ includes the effects of nonequilibrium reacting gases and can be expressed in several different forms, but one convenient form for numerical computation is

$$G = -w_O/c_{pf}[\tfrac{3}{2}R + D/T - R\theta_v/T(e^{\theta/T} - 1) - c_{pf}/(1 + \alpha)] \quad (8)$$

where c_{pf} is the specific heat at constant pressure and composition,

$$c_{pf} = \partial h/\partial T)_{P,\alpha} = [(7 + 3\alpha)/2]R + (1 - \alpha)R\theta_v^2 e^{\theta_v/T}/T^2 \times (e^{\theta_v/T} - 1)^2 \quad (9)$$

The term w_O, the net mass rate of production of atoms, will be algebraically defined by Eq. (12). The sound speed a in Eqs. (7) is that at frozen composition (see Ref. 13) and is given by

$$a^2 = \partial P/\partial\rho)_{s,\alpha} = \{[c_{pf}/c_{pf} - R(1 + \alpha)]\}(1 + \alpha)R'T$$

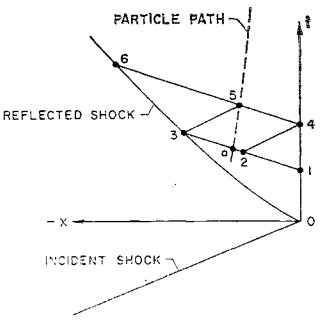

Fig. 2 Characteristic network construction.

Consideration of nonequilibrium reacting flows complicates the method of characteristics in that changes in concentration and entropy occur along particle paths, i.e., streamlines. A determination of the conditions at a given point in a flowfield must therefore account for these variations as well as for those changes in pressure and velocity prescribed by Eqs. (7). Along a particle path, differences in composition and entropy are given by

$$\delta\alpha/\delta t = w_O/\rho \quad (10)$$

and

$$\frac{\delta S}{\delta t} = -\frac{1}{\rho T}\sum_k \mu_k w_k \quad (11)$$

where k represents a specific chemical species, in this case O or O_2. The quantity w_O, the net mass rate of production of atoms, is given by

$$w_O = -Wk_r(-K_c[O_2][X] + [O]^2[X]) \quad (12)$$

The chemical potentials appearing in Eq. (11) are taken to be of the following form:

$$\mu_O = -(2RT/W)\ln[14.419(T^{5/2}/p_O)e^{-\theta_d/2T}] \quad (13)$$

$$\mu_{O_2} = -\frac{RT}{W}\ln\left[3.714\,\frac{T^{7/2}}{p_{O_2}}\,\frac{1}{1 - e^{-\theta_v/T}}\right] \quad (14)$$

where p_O and p_{O_2} are the partial pressures, and, of course,

$$w_O = -w_{O_2} \quad (15)$$

Logic of numerical solution

The present solution, in common with all characteristics solutions, proceeds from a set of points in the flowfield where all of the flowfield properties are known, such as points 1, 2, and 3 of Fig. 2. The properties at each new point along a subsequent ray (points 4, 5, and 6) are computed in two steps. First, the pressure and particle velocity are found by an appropriate simultaneous solution of Eqs. (7a) and (7b) (subject to boundary conditions imposed at shock-wave and end-wall points). Secondly, the remaining properties at the new point are found by integrating Eqs. (10) and (11) along the particle path that passes through the new point (see Fig. 2). Continuation of the solution is accomplished by successive computation of rays.

The conditions along an initial ray, e.g., points 1, 2, and 3 are found from a starting approximation. First, the conditions at the point of reflection are calculated assuming equilibration of vibrational energy but frozen chemistry across the reflected shock wave. Next, the properties at point 1 are established assuming the pressure and enthalpy remain constant for a very short time along the end wall. Finally, the conditions at point 3 are found from a simultaneous solution of Eq. (7b) and the appropriate shock-jump relations. Conditions at point 2 are simply interpolated between the conditions at points 1 and 3.

Although the brief description provided here is for a fixed number of points along each ray, additional points are added

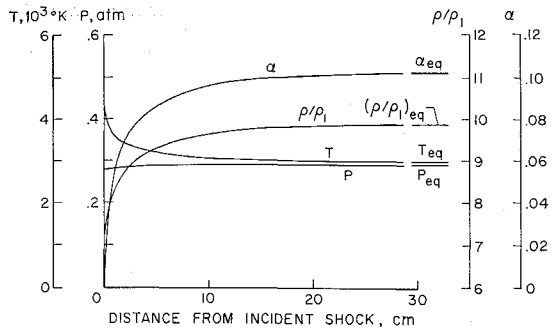

Fig. 3 Incident-shock flowfield profiles for case I.

(by interpolation) along each successive ray to keep the mesh sufficiently small to preserve accuracy. Furthermore, in order to obtain good accuracy and stability in the region immediately behind the reflected shock wave, where very large property gradients are present, a fine mesh is incorporated into this region of the network. The number of points in this fine mesh is variable and depends upon the magnitude of the property gradients. As a further preventive of errors because of large property gradients, each point in the entire flowfield is iterated once by averaging the properties of the calculated point with those of the known points, assigning the averaged values to the coordinates of the known points and recomputing the unknown point. In addition, Eqs. (10) and (11) are integrated along each particle path by assuming a linear variation in pressure and dividing each major interval, such as from point a to point 5 of Fig. 2, into 20 small intervals for numerical integration.

Results and Discussion

Several solutions of reflected-shock flowfields have been obtained, and the initial conditions for these solutions are summarized in Table 1. In this paper, the results of case I will be discussed in detail. Partial results also will be presented from the four remaining cases in order to show the effect of changing the initial pressure, case II, the reaction-rate constant, case III, and the incident-shock velocity, cases IV and V. The results of the computer program lend themselves to two types of presentations, end-wall properties ($x = 0$) as a function of time and flowfield properties as a function of x for discrete times.

Profiles of flowfield properties for the incident-shock nonequilibrium solution are shown in Fig. 3 as a function of distance behind the shock wave; convergence to the limiting equilibrium conditions is apparent. The solution is typical of the dissociative relaxation of a diatomic gas and the relevant details will be recalled when pertinent in the following discussion.

Variations in several end-wall properties as a function of time are shown in Fig. 4. The most striking departure from the typical behavior exhibited in an incident-shock flow-

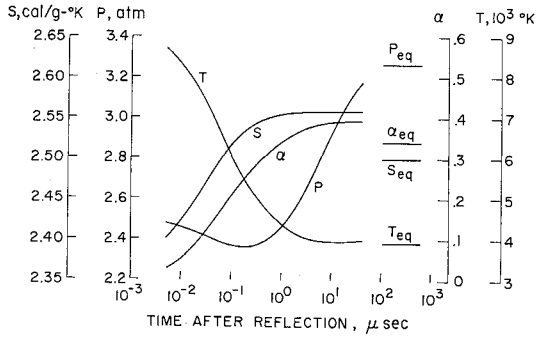

Fig. 4 End-wall properties as a function of time after reflection, case I.

Table 1 Summary of computer solutions

Case	U, km/sec	P_1, atm	β
I	3.05	2.63×10^{-3}	1
II	3.05	13.15×10^{-3}	1
III	3.05	2.63×10^{-3}	5
IV	3.96	2.63×10^{-3}	1
V	2.01	2.63×10^{-3}	1

field is evident in the pressure history. Whereas the pressure behind the incident-shock wave is nearly constant (see Fig. 3), the pressure behind the reflected-shock wave first decreases in a comparatively short time span and then increases over a much longer time period. The initial decrease in pressure may be attributed to the fast chemical relaxation behind the reflected shock wave, whereas the increase in pressure is a consequence of the slower relaxation behind the incident-shock wave.

In the case exhibited here, the relaxation time behind the incident-shock wave is much longer than the relaxation time behind the reflected shock. The gas in the reflected region thus quickly relaxes toward a state of local thermodynamic equilibrium corresponding to chemically frozen flow behind the incident shock and chemical equilibrium behind the reflected shock. The pressure for such a condition is less than that corresponding to frozen chemistry behind both the incident- and reflected-shock waves since the effect of increasing density in the reflected region (due to dissociation) must be to decrease the reflected-shock-wave velocity and hence to decrease its corresponding pressure jump.

The slow increase in pressure toward the "equilibrium" value is due to the nonequilibrium flow behind the incident-shock wave. (Herein, an "equilibrium" value is defined as the magnitude of a flowfield property when calculated assuming complete and instantaneous thermodynamic equilibrium behind both the incident- and reflected-shock waves; this is the value usually tabulated in tables of reflected-shock properties for real gases.) In fact, to a first approximation the pressure rise at the end wall occurs with the same time scale and in direct proportion to the density variation behind the incident-shock wave. This observation becomes apparent if one recognizes that the end wall effectively samples the incident-shock dynamic pressure, which increases with distance behind the incident-shock wave. A consequence of this large pressure variation is that the end-wall pressure now becomes an attractive observable for reaction-rate studies. Similar behavior of the end-wall pressure was previously noted by Baganoff,[9] and demonstrated by Johannesen et al.,[10] for shock-wave reflection in vibrationally relaxing CO_2.

The temperature at the end wall has an initial value corresponding to frozen flow behind both the incident- and reflected-shock waves. However, as the relaxation proceeds, the temperature is seen to decrease rapidly toward the

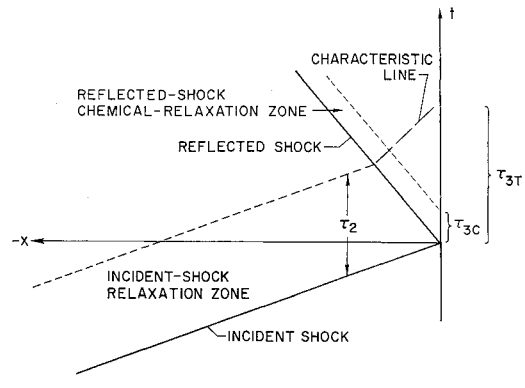

Fig. 5 Graphic description of controlling times for reflected-shock-wave relaxation.

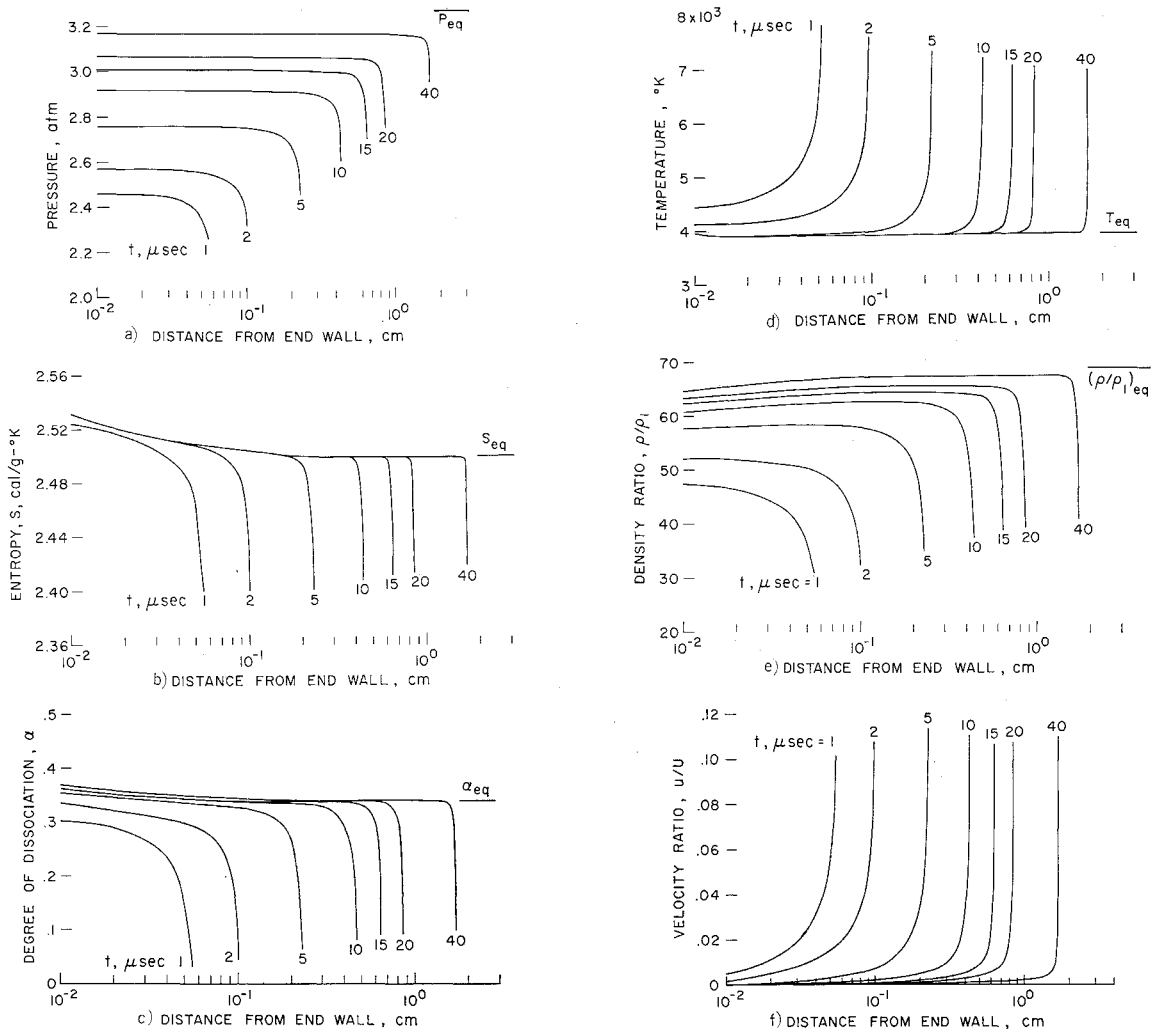

Fig. 6 Flowfield properties as a function of distance from the end wall for discrete times after reflection, case I: a) pressure, b) entropy, c) degree of dissociation, d) temperature, e) density, and f) flow velocity relative to end wall.

equilibrium value, and then increase toward a final steady-state value. The presence of two time scales can be seen in that the temperature approaches a minimal value in a time that is much less than that required for the pressure to approach its steady-state value. The time required for the temperature to approach its minimal value τ_{3c} can be considered as the chemical relaxation time behind the reflected-shock wave, and also is evident in the relaxation of other variables, such as α and S, which are sensitive to chemical processes.

A further consequence of the nonsteady nature of shock-wave reflection in a relaxing gas is evident in the behavior of S, α, and T for long times on the end wall. It can be seen that all three of these properties approach steady-state values that are above their corresponding equilibrium values. Although the pressure must approach, at long times, its equilibrium value, the final steady-state solution for the other thermodynamic properties should not correspond to the usual equilibrium values. Physically, the explanation for this result is that those gas particles adjacent to the end wall are processed by a stronger reflected-shock wave and have different time histories than those particles that are processed by the eventual equilibrium-strength reflected-shock wave. Table 2 gives a summary of the end-wall values at 41.4 μsec, at which time the solution was terminated because of excessive computer time (approximately 6 hrs on an IBM 7094 computer).

Table 2 Comparison of end-wall solutions

	P, atm	T, °K	S, cal/g-°K	α	ρ/ρ_1
Noneq. sol.	3.176	3994	2.558	0.393	63.80
Eq. sol.	3.268	3919	2.501	0.342	69.39
Ratio ≡ noneq./eq.	0.97	1.02	1.02	1.15	0.92

To summarize the information presented in Fig. 4, the steady-state values on the end wall, for all of the thermodynamic properties except pressure, do not correspond to the usual equilibrium values. Also, the relaxation of the flow appears to be controlled by two separate relaxation times. The first, τ_{3c}, is a consequence of the chemical relaxation behind the reflected-shock wave. The second, τ_{3T}, the time for the pressure to reach a steady-state condition, is controlled by the relaxation time behind the incident-shock wave τ_2; and τ_{3T} is approximately equal to τ_2. A graphic description of these characteristic times is shown in Fig. 5. It is obvious that a steady-state solution cannot be attained behind the reflected-shock wave until the right-running characteristic that originates at the intersection of the reflected-shock wave and the end of the incident-shock relaxation zone, a loosely defined point, reaches the end wall.

Flowfield properties P, S, α, T, ρ/ρ_1, and u/U are presented in Figs. 6a–6f as a function of distance from the end wall for discrete times after shock reflection. These plots are essentially "snapshots" of the various properties in the entire reflected-shock flowfield taken at various intervals of time after the instant of shock reflection. Figure 6a

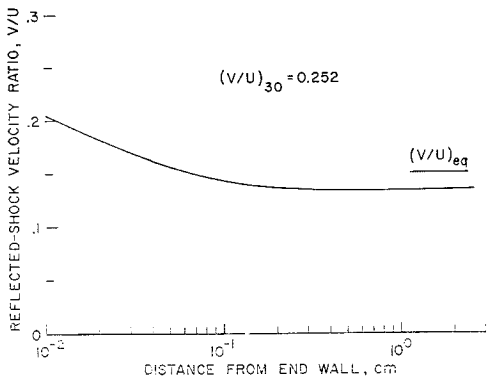

Fig. 7 Reflected-shock velocity relative to end wall, case I.

shows the variation in pressure for times between 1 and 40 μsec. It is seen that a plateau of near constant pressure develops within about 5 μsec, and that the pressure remains spatially uniform thereafter. The large pressure variation throughout the flowfield for very short times, and near the shock for longer times, is associated with the chemical relaxation behind the reflected-shock wave. The slow increase in the pressure level of the plateau is associated with the chemical relaxation behind the incident-shock wave. The termination of each curve represents the pressure immediately behind the reflected-shock wave.

The spatial variation in entropy behind the reflected-shock wave is shown in Fig. 6b. As pointed out in Fig. 4, the entropy at $x = 0$ quickly exceeds the equilibrium value, and it can be seen in Fig. 6b that this excess extends into the flowfield and forms a variable-entropy layer near the end wall. As the shock moves away from the end wall, this layer becomes of nearly fixed extent (see $t > 10$ μsec curves) and a steady-state entropy value is approached outside the layer that is asymptotic to the equilibrium value. The large entropy gradient near the shock wave is a consequence of the chemical relaxation behind the reflected shock.

Spatial distributions of degree of dissociation and temperature are shown in Fig. 6c and d, respectively. It is noted that after the entropy layer is fully developed, both α and T have values that are higher than their corresponding equilibrium levels. However, steady-state plateaus, wherein the properties approach their equilibrium values, begin to develop away from the end wall at times greater than about 10 μsec. The value of α immediately behind the reflected-shock wave for a time of 40 μsec is 0.099. Since no change in α occurs across the reflected shock, this value corresponds to a distance about halfway through the incident-shock nonequilibrium zone as shown in Fig. 3. This suggests that more than 80 μsec is required to obtain a near steady-state solution behind the reflected-shock wave.

The spatial variation in density is shown in Fig. 6e. A sharp decrease in density is present across the variable-entropy layer. For long times, the density is strongly coupled to pressure, so no steady-state value is approached in the time span shown on the figure. Measurements of density profiles have been used extensively to obtain rate information behind incident-shock waves. The variation in density behind the reflected-shock wave, at a fixed distance from the end wall, also could be used to infer reaction rates, but more care must be exercised in interpreting the data since the density profiles are different functions of time for different observation stations. The decrement in density because of the entropy layer near the end wall also should be detectable in a density measurement; in fact, Johannesen et al.[10] have obtained interferometer records exhibiting such a density decrease, partially masked by end-wall heat-transfer effects, for the vibrational relaxation of CO_2 behind a reflected-shock wave.

A boundary condition for equilibrium calculations behind reflected-shock waves is that the flow velocity, relative to the shock-tube end wall, vanishes throughout the flowfield. However, as mentioned earlier, for nonequilibrium calculations this boundary condition can be imposed only at the end wall. Spatial variations of u/U are shown in Fig. 6f, and it is seen that a large gradient in flow velocity exists near the shock wave. However, at a time of 40 μsec, the flow velocity approaches zero over a major portion of the flowfield. Within the variable-entropy layer, the velocity is expected to be small since the pressure gradient (spatial) is so small.

Strehlow and Cohen[5] have shown that vibrational relaxation in nitrogen and oxygen causes an initial deceleration in the velocity of the reflected shock wave, relative to the shock tube. A similar behavior is shown in Fig. 7 for the case of dissociation of a diatomic molecule. The reflected shock velocity initially (i.e., at $x = 0$) has a value corresponding to frozen chemistry with $\alpha = 0$ behind both the incident- and reflected-shock waves. However, the velocity quickly decelerates to a value that is less than the equilibrium value and corresponds closely to a condition of frozen chemistry behind the incident-shock wave and equilibrium chemistry behind the reflected-shock wave. After reaching a minimum, the reflected-shock velocity increases slowly and should eventually reach the equilibrium value.

The foregoing figures present a complete description of a nonequilibrium reflected-shock flowfield. As discussed earlier, two relaxation times control the flow behind the reflected shock. Also, a variable-entropy layer, in which the entropy (as well as the temperature and the extent of dissociation) locally exceeds the equilibrium value, is seen to develop near the end wall. The excess of entropy in this variable-entropy layer will not diminish since, within the assumptions of the present model, there is no mechanism available to drive the entropy back to its equilibrium value.

Capiaux and Washington[14] have investigated the analogous problem of nonequilibrium hypersonic flow of a dissociating gas past a semi-infinite wedge with a sharp leading edge. Their calculations also predict the formation of an entropy layer, located above the surface of the wedge, but they did not discuss the magnitude of the steady-state surface entropy in comparison to the equilibrium value. However, for their case, wherein the shock wave was convex, one also would expect that the surface entropy should exceed the equilibrium value appropriate for the deflection angle of the wedge.

If the end-wall entropy always remains higher than the equilibrium level, then attention can be focused on the magnitude of the remaining thermodynamic properties in the entropy layer as a steady-state solution is approached. It can easily be shown that the pressure must approach the equilibrium value throughout the flowfield for long times after reflection since a pressure gradient cannot be sustained in the flowfield. This comes about since, in a coordinate system that is fixed relative to the reflected shock, the flow for long times after reflection must behave similar to an incident-shock solution with upstream properties corresponding to the

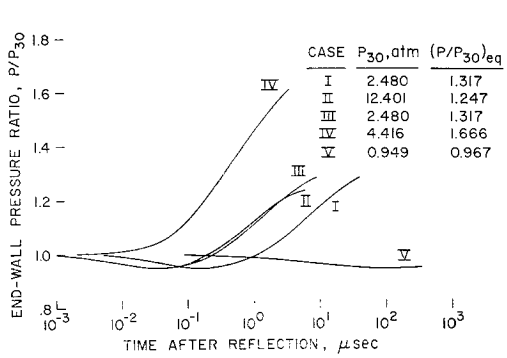

Fig. 8 Comparison of end-wall pressure histories, cases I-V.

equilibrium conditions behind the actual incident-shock wave, see Fig. 3. At the final steady-state condition, thermodynamic equilibrium must exist; therefore $DS/Dt = 0$, whereas $P = P_{3eq}$ and $S > S_{3eq}$. These results lead one to the conclusion that all of the steady-state properties within the variable-entropy layer, except pressure, will correspond to a condition of thermodynamic equilibrium different from the usual equilibrium properties.

It has been shown, in Fig. 4, that large variations in end-wall pressure are present during shock-wave reflection. Since pressure is a convenient experimental measurable, the sensitivity of end-wall pressure to experimental parameters and the chemical reaction rate is of importance in determining its suitability as a diagnostic in reaction-rate studies. End-wall pressure histories are shown in Fig. 8 for all of the solutions that have been obtained. Case I is used as the standard and all comparisons are made with reference to its end-wall pressure history. The pressure coordinate has been normalized by the frozen reflected-shock pressure for each solution. All of the solutions were terminated prior to reaching steady-state solutions due to the use of excessive computer time.

Case II represents a fivefold increase in P_1, while holding the incident-shock velocity and reaction-rate parameters constant. The over-all shape of the end-wall pressure history is essentially the same as for case I, but, as would be expected, the time to approach a steady state is decreased by about a factor of 5. Case III shows the effect of increasing the reaction rate by a factor of 5 while holding the initial pressure and incident-shock velocity the same as for case I. As might be expected, the time scale of the pressure variation has been reduced by exactly a factor of 5, indicating that the entire characteristics solution scales inversely with the rate-constant multiplier. Since the histories for cases II and III are not coincident, it should be pointed out that binary scaling is only approximately obeyed. These results confirm that the end-wall pressure is a sensitive observable for reaction-rate studies.

Cases IV and V show the effect of changing the incident-shock velocity, while holding the initial pressure and reaction rate the same as for case I. These cases point out the limiting effects of strong and weak interactions with the incident-shock flowfield. As can be seen from the end-wall pressure history of case I, two competing effects are present. First, the chemical relaxation behind the reflected-shock wave introduces a negative pressure gradient in time (with a time scale τ_{3c}) as the flow relaxes from frozen to equilibrium chemistry. Secondly, the gradient in flow properties behind the incident-shock wave induces a positive pressure gradient (with an approximate time scale τ_2) on the end wall. Case IV represents a solution wherein the initial values of these two gradients nearly cancel and no dip in pressure occurs on the end wall, i.e., there is a strong interaction with the incident-shock flowfield. A strong interaction thus occurs when the relaxation times τ_{3c} and τ_2 are not widely separate. Case V shows the result of a weak interaction where the overriding effect is the negative gradient due to chemical relaxation behind the reflected-shock wave, and only a slight positive gradient appears near the end of the solution. This case corresponds closely to a situation wherein there is no chemical relaxation behind the incident-shock wave and hence the relaxation times are very widely separate. In general, the strength of the interaction increases (i.e., the relaxation times become less widely separate) as shock speed increases. The critical speed at which the initial pressure gradient is zero depends on the reaction rates chosen (in particular on their temperature dependence); for the rates used here the critical speed corresponds closely to case IV.

Concluding Remarks

In contrast to nonequilibrium incident-shock flowfields, a large variation in pressure may be present behind reflected-shock waves. The magnitude of this pressure change, and the sensitivity of its time scale to experimental variables, make it an attractive observable for reaction-rate studies.

The relaxation process behind a reflected-shock wave exhibits two separate time scales. Properties that are sensitive to the chemical state, such as entropy, temperature, and the degree of dissociation, relax in a time τ_{3c} that is controlled by the chemical reaction rate behind the reflected-shock wave. Properties that are sensitive to fluid-dynamic phenomena, such as pressure and density, relax in a time τ_{3T} that is controlled by the time to obtain steady-state conditions behind the incident shock wave, and τ_{3T} is usually much greater than τ_{3c}.

A variable-entropy layer of gas is formed, adjacent to the end wall, in which all of the thermodynamic properties, except pressure, differ significantly from their usual equilibrium conditions as a steady-state solution is approached.

References

[1] Johnson, C. D. and Britton, D., "Shock Waves in Chemical Kinetics: The Use of Reflected Shock Waves," *Journal of Chemical Physics*, Vol. 38, No. 7, April 1, 1963, p. 47.

[2] Kamimoto, G., Akamatsu, T., and Hasegawa, T., "Effect of Shock Attenuation on Reflected Shock Waves," CP2, Oct. 1962, Department of Aerospace Engineering, Kyoto Univ., Japan.

[3] Rudinger, G., "Effect of Boundary-Layer Growth in a Shock Tube on Shock Reflexion From a Closed End," *The Physics of Fluids*, Vol. 4, No. 12, Dec. 1961, p. 1463.

[4] Mark, H., "The Interaction of a Reflected Shock Wave with the Boundary Layer in a Shock Tube," TM 1418, March 1958, NACA.

[5] Strehlow, R. A. and Cohen, A., "Limitation of the Reflected Shock Technique for Studying Fast Chemical Reactions and its Application to the Observation of Relaxation in Nitrogen and Oxygen," *Journal of Chemical Physics*, Vol. 30, No. 1, Jan. 1959, p. 257.

[6] Lin, S. C. and Fyfe, W. I., "Low-Density Shock Tube for Chemical Kinetics Studies," *The Physics of Fluids*, Vol. 4, No. 2, Feb. 1961, p. 238.

[7] Sturtevant, B. and Slachmuylders, E., "End Wall Heat-Transfer Effects on the Trajectory of a Reflected Shock Wave," *The Physics of Fluids*, Vol. 7, No. 8, Aug. 1964, p. 1201.

[8] Goldsworthy, F. A., "The Structure of a Contact Region, with Application to the Reflexion of a Shock from a Heat Conducting Wall," *Journal of Fluid Mechanics*, Vol. 5, 1959, p. 164.

[9] Baganoff, D., "Experiments on the Wall-Pressure History in Shock-Reflexion Processes," *Journal of Fluid Mechanics*, Vol. 23, Pt. 2, 1965, p. 209.

[10] Johannesen, N. H., Bird, G. A., and Zienkiewicz, H. K., "Theoretical and Experimental Investigations of the Reflexion of Normal Shock Waves with Vibrational Relaxation," *Journal of Fluid Mechanics*, Vol. 30, Pt. 1, 1967, p. 51.

[11] Greene, E. F. and Toennies, J. P., *Chemical Reactions in Shock Waves*, Academic Press, New York, 1964.

[12] Ferri, A., *Fundamental Data Obtained From Shock Tube Experiments*, Pergamon Press, New York, 1961.

[13] Chu, B. T., "Wave Propagation and the Method of Characteristics in Reacting Gas Mixtures with Applications to Hypersonic Flow," TN 57-213, May 1957, Wright Air Development Center, Wright-Patterson Air Force Base, Ohio.

[14] Capiaux, R. and Washington, M., "Nonequilibrium Flow past a Wedge," *AIAA Journal*, Vol. 1, No. 3, March 1963, pp. 650–660.